Astron. Astrophys. 362, 333–341 (2000)

ASTRONOMY AND ASTROPHYSICS

The distribution of shock waves in driven supersonic turbulence

M.D. Smith[1], **M.-M. Mac Low**[2], **and F. Heitsch**[3]

[1] Armagh Observatory, College Hill, Armagh BT61 9DG, Northern Ireland, UK (mds@star.arm.ac.uk)
[2] Department of Astrophysics, American Museum of Natural History, 79th St. at Central Park West, New York, NY 10024-5192, USA (mordecai@amnh.org)
[3] Max-Planck-Institut für Astronomie, Königstuhl 17, 69117 Heidelberg, Germany (heitsch@mpia-hd.mpg.de)

Received 15 May 2000 / Accepted 3 August 2000

Abstract. Supersonic turbulence generates distributions of shock waves. Here, we analyse the shock waves in three-dimensional numerical simulations of uniformly driven supersonic turbulence, with and without magnetohydrodynamics and self-gravity. We can identify the nature of the turbulence by measuring the distribution of the shock strengths.

We find that uniformly driven turbulence possesses a power law distribution of fast shocks with the number of shocks inversely proportional to the square root of the shock jump speed. A tail of high speed shocks steeper than Gaussian results from the random superposition of driving waves which decay rapidly. The energy is dissipated by a small range of fast shocks. These results contrast with the exponential distribution and slow shock dissipation associated with decaying turbulence.

A strong magnetic field enhances the shock number transverse to the field direction at the expense of parallel shocks. A simulation with self-gravity demonstrates the development of a number of highly dissipative accretion shocks. Finally, we examine the dynamics to demonstrate how the power-law behaviour arises.

Key words: hydrodynamics – shock waves – turbulence – ISM: clouds – ISM: kinematics and dynamics

1. Introduction

Many structures we come across in the Universe have been shaped by fluid turbulence. In astronomy, we often observe high speed turbulence driven by supersonic ordered motions such as jets, supernova shocks, galactic rotation and stellar winds (e.g. Franco & Carramiñana 1999). Although it has long been thought that astrophysical turbulence provides the best opportunity to investigate supersonic turbulence, the lack of a theory has stunted our attempts to understand the behaviour (von Hoerner 1962). Three dimensional high resolution numerical simulations now provide a method to make real progress. Driven turbulence is explored in this paper and the results compared to a sister study of decaying turbulence (Smith et al. 2000, hereafter Paper 1). Our aim here is to relate the type of turbulence to the properties of the shock waves.

We study here compressible turbulence without thermal conduction. No physical viscosity is modelled, but numerical viscosity remains present, and an artificial viscosity determines the dissipation in regions of strong convergence. Periodic boundary conditions were chosen for the finite difference ZEUS code simulations, fully described by Mac Low et al. (1998). Uniform three dimensional turbulence with an isothermal equation of state, an initially uniform magnetic field and periodic boundary conditions are investigated. The influence of self-gravity is also examined.

Our motivation here is to provide the observer with a means of recognising the type of turbulence from the properties of the generated shock waves. The general energetics of decaying and driven hydrodynamic turbulence have already been computed by Mac Low et al. (1998) and Mac Low (1999), respectively, using ZEUS, a second-order, Eulerian hydrocode. Mac Low et al. (1999) concluded that, since turbulence which is left to decay dissipates rapidly under all conditions, the motions we observe in molecular clouds must be continuously driven. Klessen et al. (2000) extended the hydrodynamic results by calculating self-gravitating models. A smoothed particle hydrodynamics (SPH) code was also employed to confirm the results for both the decaying and driven cases (Mac Low et al. 1998, Klessen et al. 2000). Klessen et al. (2000) have provided the parameter scaling for applications to molecular clouds. Heitsch et al. (2000) present the magnetohydrodynamic extension to the self-gravitating case, and discuss the criteria for gravitational collapse.

Our immediate target is to derive the spectrum of shocks (the Shock Probability Distribution Function) generated by driven turbulence. With this knowledge, we will proceed to predict the spectroscopic properties in a following work. Observed individual bright, sharp features, such as arcs, filaments and sheets, are often interpreted as shock layers within which particles are highly excited (e.g. Eislöffel et al. 2000). Where unresolved, the excitation can still be explored quantitatively by employing spectroscopic methods. The gas excitation then depends on both the physics of shocks as well as the distribution of shock strengths.

Send offprint requests to: M.D. Smith

Previous studies of compressible turbulence have concentrated on the density and velocity structure of the cold gas rather than the shocks (e.g. Porter et al. 1994; Falgarone et al. 1994, Vázquez-Semadeni et al. 1996, Padoan et al. 1998). This may be appropriate for the interpretation of clouds since, although the Mach number is still high, the shock speeds are too low to produce bright features. The simulations analysed here are also being interpreted by Mac Low & Ossenkopf (2000) in terms of density structure.

The method used to count shocks from grid-based simulations was developed in Paper 1. The one-dimensional counting procedure was verified through a comparison with full three-dimensional integrations of the dissipated energy in Paper 1. This method is appropriate for a ZEUS-type finite difference code for which shock transitions are spread out over a few zones. Here, we also study the shock transitions in all three directions and display the spatial distributions for the energy dissipated through the artificial viscosity in the shocks. We first present the shock jump PDFs and provide analytical fits (Sect. 2). Magnetohydrodynamic simulations (Sect. 3) with Alfv́en numbers of $A = 5$ and $A = 1$ are then explored. Note the definition of the Alfvén Mach number $A = v_{\rm rms}/v_A$, where the Alfvén speed $v_A = (B^2/4\pi\rho)^{1/2}$, and $v_{\rm rms}$ is the initial root mean square (rms) velocity.

Which shocks actually dissipate most of the energy? The shock power rather than number density will determine the spectral region in which the system can be best observed. Hence, we determine the energy dissipated as a function of the shock speed in Sect. 4. A large-scale simulation which included self-gravity is then analysed in Sect. 5. We next interpret the results in terms of the dynamical models (Sect. 6).

2. Hydrodynamic turbulence

2.1. Model description

We first explore driven hydrodynamic turbulence. The three-dimensional numerical simulations on grids with 128^3 and 256^3 zones and periodic boundary conditions were initialized with an rms Mach number of $M = 5$. The initial density is uniform and the initial velocity perturbations were drawn from a Gaussian random field, as described by Mac Low (1999). The power spectrum of the perturbations is flat and limited to small wavenumber ranges, $k_{\rm min} < k < k_{\rm max}$, with $k_{\rm min} = 7$ and $k_{\rm max} = 8$ in Fig. 1. The uniform driver is a simple constant rate of energy input with the distribution pattern fixed.

The simulations employ a box of length $2L$ and a unit of speed, u. The gas is isothermal with a sound speed of $c_s = 0.1\,u$. Hence the sound crossing time is 20 L/u. We take the time unit as $\tau = L/u$. Assuming a mass m to be contained initially in a cube of side L, the dissipated power is given in units of $\dot{E}_o = mu^2/\tau$.

2.2. Shock number distribution

We calculate the one dimensional shock jump function, as discussed and justified in Paper 1. This is the number distribution of the total jump in speed across each converging region along a specific direction. This is written as dN/dv_j where v_j is the sum of the (negative) velocity gradients (i.e. $\Sigma\,[-\delta v_x]$ across a region being compressed in the x-direction). We employ the jump Mach number in the x-direction $M_j = v_j/c_s$ rather than v_j since this is the parameter relevant to the dynamics. Thus, each bounded region of convergence in the x-direction counts as a single shock and the total jump in M_j across this region is related to its strength.

Numerically, we scan over the whole simulation grid (x,y,z), recording each shock jump through

$$M_j = \sum_{x=x_i}^{x=x_f} (\Delta v_x/c_s) \tag{1}$$

with the condition that $\Delta v_x < 0$ in the range $x_i \le x < x_f$. This is then binned as a single shock element. The shock number distribution dN/dM_j is obviously dimensionless.

Note that the shock number depends on the grid size. We find that on doubling the grid size, the shock number increases by a factor of four. This implies that the total shock front *area* in units of L^2 remains roughly constant. This holds for both driven and decaying turbulence and is an indication that the numerical resolution is sufficient to capture the vast majority of shocks.

2.3. Steady state description

The random Gaussian field at t = 0 rapidly transforms into a shock field (Fig. 1). As can be seen, the shock distribution approaches a steady state, reached by t = 1. The driving energy determines the break in the distribution and the maximum shock speed, but does not influence the *distribution* of shock speeds.

The driving wavenumber influences the steady state as shown in Fig. 2. There is a moderate dependence of the shock number on the wavenumber, especially at high Mach numbers. This may be partly due to the time involved for the regenerated low wavenumber modes to steepen. Some of the longer wave modes may be damped by interactions with the turbulent field.

A power law distribution of shock velocities is uncovered. Note that for high Mach numbers, statistically, we can equate the shock Mach number to the jump Mach number to a good approximation. We find, as shown by the indicated line in the lower box of Fig. 1, an inverse square-root law $dN/dM_j \propto M_j^{-0.5}$. In detail, we find a fit of the form

$$\frac{dN}{dM_j} \sim 1.4\,10^4\,k^{0.5}\,\dot{E}^{-0.2}\,M_j^{-0.5} \tag{2}$$

over the power law sections. The break in the power law is found to occur at M_j^{max} given by

$$M_j^{max} \sim 7.6\,k^{0.2}\,\dot{E}^{0.4}. \tag{3}$$

The k-dependence for M_j^{max} has been estimated by inspecting the energy dissipation diagrams below. The indicated value is consistent with that discernable in Fig. 2.

Integrating Eq. (2), using the limit Eq. (3), yields the remarkable result that the number of shocks is a constant: $N \sim 178,000$ for $k = 8$. That is, when the energy input is low, there are many

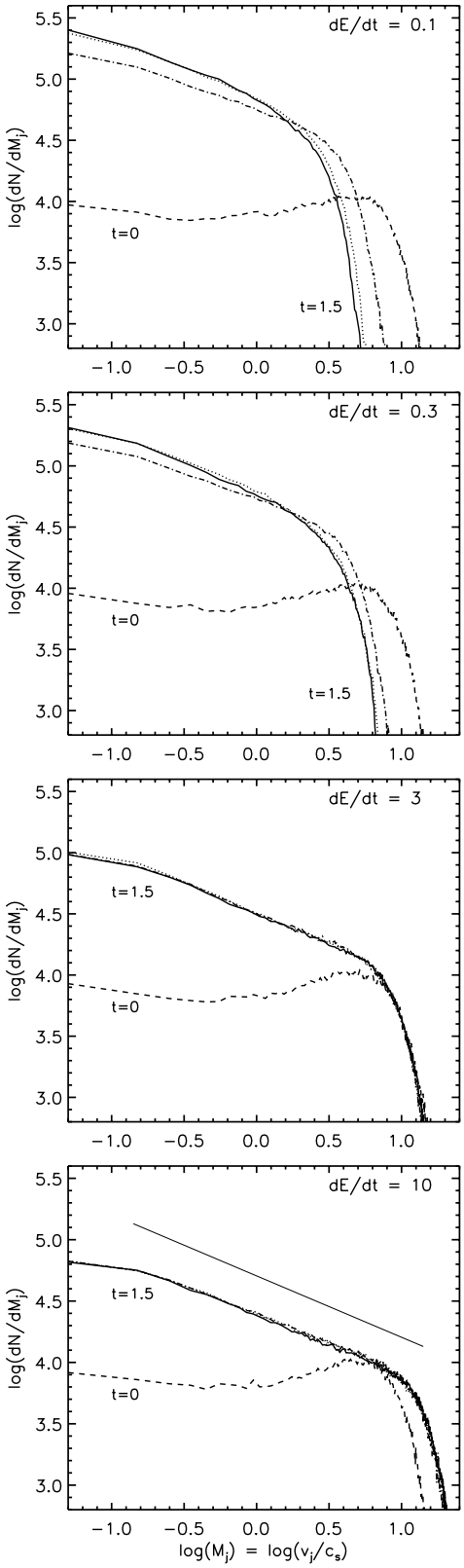

Fig. 1. Four simulations of driven hydrodynamic turbulence with an increasing rate of energy input from top to bottom. The distribution of jumps are shown at four times for each simulation, from t=0 (dashed), t=0.5 (dot-dash), t=1.0 (dotted) to t=1.5 (solid). The thin straight line in the lower panel represents an inverse square root law.

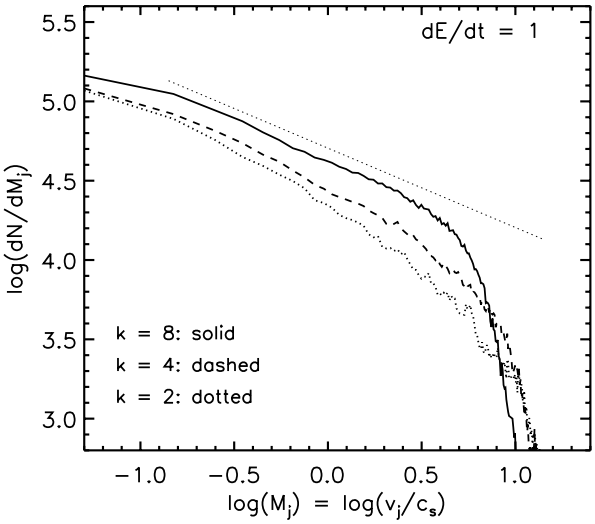

Fig. 2. The shock distribution depends on the wavenumber of the energy input of the driven hydrodynamic turbulence. The straight dotted line has the slope given by Eq. (2).

more weak shocks. As the energy is increased, the number of shocks does not increase. Rather, the shock strengths increase. Hence, the number of shocks reaches a saturation level of about 180,000 on the 128^3 grids.

Hence, the total shock surface area is $N \propto k^{0.4}$. This is confirmed directly from the shock counts. We find that the number of jumps does depend weakly on the chosen value for the minimum convergence. We take the case $dE/dt = 10$ for illustrative numbers. Taking all converging flow regions, yields 181,000 shocks with 5.17 zones per shock. This gives 46% of the volume occupied by converging regions. Taking instead a minimum convergence of $0.5\,c_s$ as a criteria which relates to a steepened wave balanced by artificial viscosity, yields 161,000 regions with an average of 3.95 zones. That is, almost 90% of the converging regions are indeed associated with steepened waves, which occupy a constant 30% of the volume. This number density was also found in decaying turbulence: even though the shocks may weaken and interact, the total number is conserved, and the total shock area is independent of the grid size (Paper 1).

Many predictions and analytical fits to simulations have been published for the velocity gradients within turbulent flows. Here, for supersonic turbulence, we find a Gaussian high-speed tail to the shock distribution provides a rough fit. Fig. 3 displays a combined power-law and Gaussian fit of the form

$$\frac{dN}{dM_j} \sim 1.4\,10^4\,k^{0.5}\,\dot{E}^{-0.2}\,M_j^{-0.45}\,\exp\left[-(M_j/15.1)^2\right] \quad (4)$$

for one case. To test if this is due to the initial Gaussian field we have also run a simulation with an exponential driver and found that a similar tail is still present. Hence the near-Gaussian could be due to the superposition of the initially randomly-located

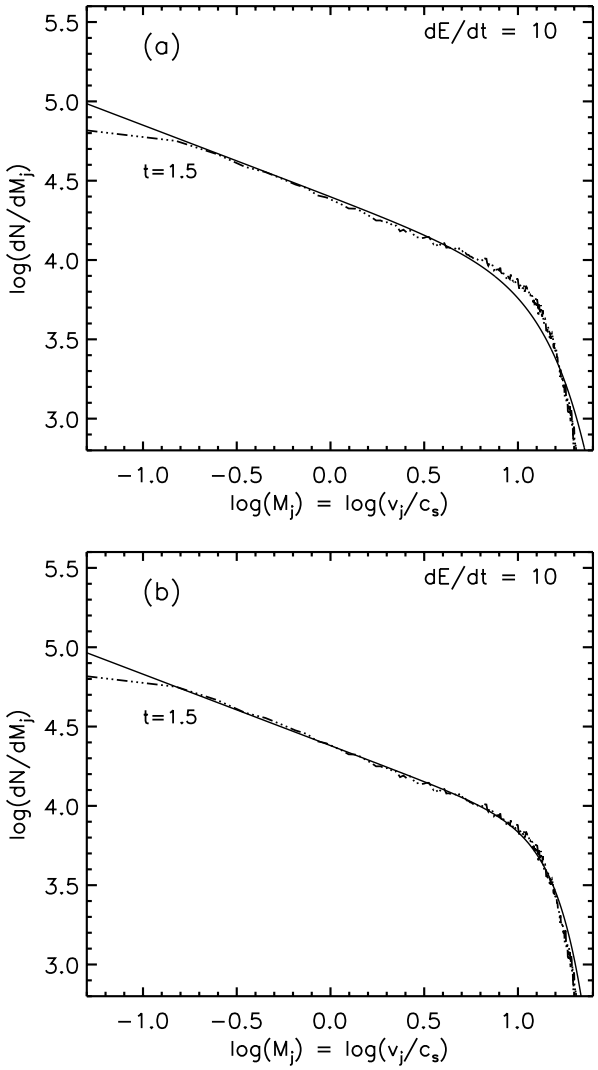

Fig. 3a and b. Power law fits combined with a **a** Gaussian tail and **b** a steep exponential tail of the form $\exp\left[-(M/16.6)^3\right]$ to the shock number distribution for the case $k = 8$ and $\dot{E} = 10$.

forcing waves, as expected from the Central Limit Theorem. The best fit we find, however, involves a tail of the form $\exp(-M^3)$,

$$\frac{dN}{dM_j} \sim 1.4\,10^4\,k^{0.5}\,\dot{E}^{-0.2}\,M_j^{-0.45}\,\exp\left[-(M_j/16.6)^3\right]. \quad (5)$$

Such steep tails have indeed been commonly found despite Gaussian driving, thought to be due to the more rapid decay of the faster shocks (e.g. Gotoh & Kraichnan 1998).

3. Magnetohydrodynamic turbulence

We introduce a uniform magnetic field into the initial configuration. A weak field, in which the Alfvén and sound speeds are equal, has little overall influence (Fig. 4). The shock distribution is roughly isotropic and the shock number is not significantly altered from the equivalent hydrodynamic simulation. The power law section is not so well defined for the shock distribution parallel to the field.

A strong field introduces a strong anisotropy (Fig. 5). With a field such that the Alfvén speed equals the initial rms speed, *the waves transverse to the field dominate*. There are $\sim$ 2–3 times more waves in the transverse direction for a given jump speed in each direction. The inverse square root power-law rule is again closely obeyed. We call these waves, rather than shocks, since the high Alfvén speed implies that a high fraction may be fast magnetosonic waves. The average number of zones, however, measured for each jump is only 4.7 (parallel) and 7.4 (transverse). This compares to an average of 5.4 for the hydrodynamic flow (and 23.7 zones for the initial Gaussian with k=4). Note these refer to the complete shock, not just the 2–3 zones across which the jump is highly non-linear and across which numerical viscosity is strong; there usually exists one or two zones on each side of the main jump across which the velocity joins smoothly onto the surrounding flow without oscillations. Hence, the zone measurements favour the interpretation that the dissipation is being carried out in short-wavelength non-linear magnetosonic waves.

A very similar difference between parallel and transverse shock numbers is found in the case of decaying turbulence (Paper 1). It is clear that the magnetic pressure is not damping the shock waves. In contrast, the extra magnetic energy which becomes tied up in the waves also helps maintain them.

4. Energy dissipation

The increasing number of strong shocks with increasing wavenumber is qualitatively consistent with the finding of Mac Low (1999) that the total energy dissipation rate increases with the driving wavenumber. To discuss the energy dissipation rate, however, we must first also consider the density ρ within each shock. We have then calculated the power dissipated by artificial viscosity within each shock front, as described in Paper 1. This yields the power dissipated per unit shock speed. We actually calculate in this section the component of the dissipation along the x-axis and the jump Mach number along the x-axis which, given the statistics, represents the true three dimensional 'power distribution function'. Numerically, over the whole simulation grid (x,y,z), we identify each compact range $x_i \le x < x_f$ along the x-axis for which $\Delta v_x = v_{x+1} - v_x < 0$. For each jump we then find the energy dissipated by artificial viscosity as

$$P_j = \frac{C}{L^2} \sum_{x=x_i}^{x=x_f} \rho_x (\Delta v_x)^3, \quad (6)$$

where C measures the number of zones over which artificial viscosity will spread a shock. This is then binned as a single shock element. The shock number distribution dP/dM_j is multiplied by three to account for the energy dissipated in each of the three dimensions. Further details of the method can be found in Paper 1, where its reliability was also verified.

The surface brightness of the shocks, as well as the column density of all the gas within the cube, is displayed in Fig. 6 for a pure hydrodynamic driven example. Note that these are not slices, but we have integrated through the z-direction. Much of

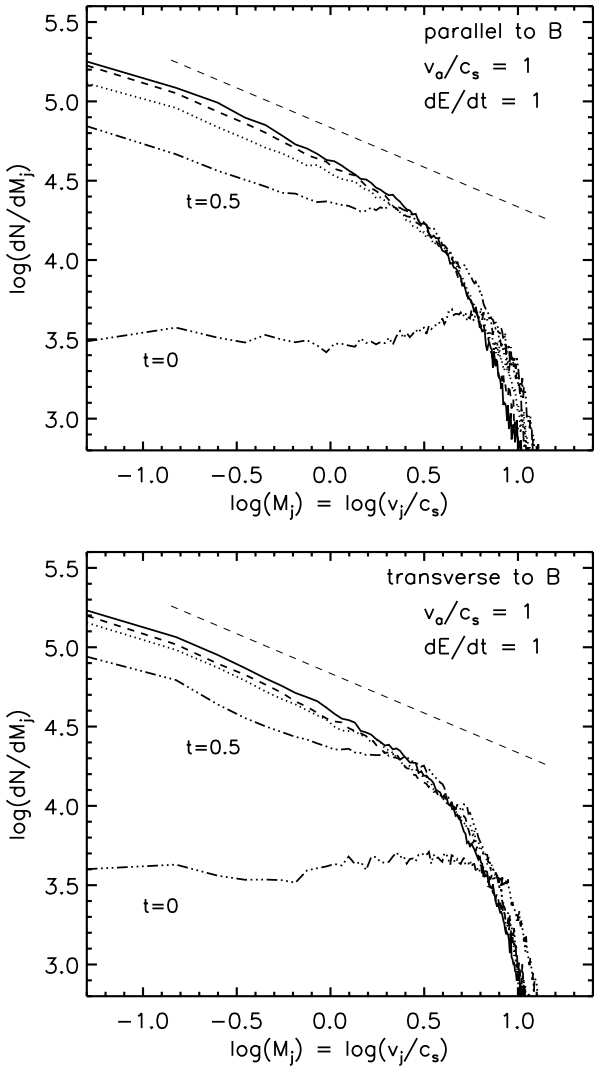

Fig. 4. The distribution of shocks in driven MHD turbulence with a 'weak' magnetic field. The shock numbers are shown here parallel and transverse to the field, at times t=0, t=0.5 (dot-dash), t=1.0 (dotted) to t=1.5 (dashed) and the time t=3.0 (solid), by which time a statistical steady state has been reached. The driving wavenumber is $k = 4$. The straight dashed line represents an inverse square root power law.

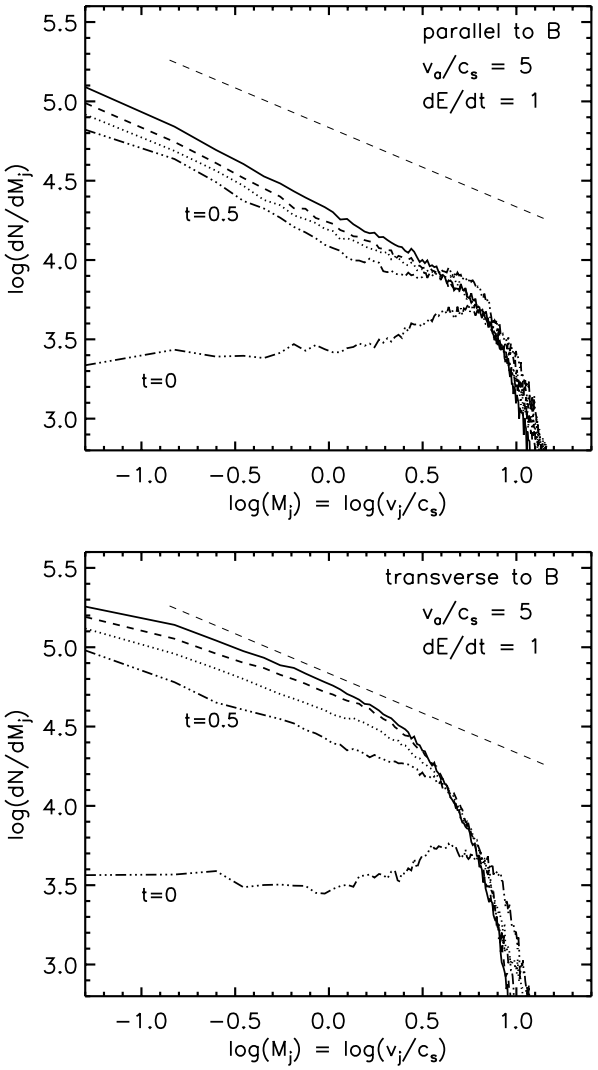

Fig. 5. The distribution of shocks in driven MHD turbulence with a strong magnetic field. The shock numbers are shown here parallel and transverse to the field, at times t=0, t=0.5 (dot-dash), t=1.0 (dotted) to t=1.5 (dashed) and the time t=3.0 (solid), by which time a statistical steady state has been reached.

the gas has been swept up into a flattened cloud. Many shocks appear sharper when only the x-direction is accounted for since this emphasizes the shocks transverse to the line of sight.

Dissipating shocks and the density distribution do not correlate very well, although the main cloud contains the main elongated region of dissipation. The most powerful shocks are mainly within the cloud.

We find that the energy dissipation rate also takes on a power law M_j dependence (Fig. 7). In contrast to the number distribution, it is independent of the driving power input. There is also a wavenumber dependence, as shown in Fig. 8.

The total energy dissipated in the power law section (summing the losses for each direction) can be written

$$\frac{dP}{dM_j} \sim 1.05\,10^{-2}\,k^{0.5}\,M_j^{1.5}. \qquad (7)$$

The error in the power law index of 1.5 is ~ 0.12. The break in the power law is found to occur at M_j^{max} as given by Eq. (3). Integrating Eq. (7), we obtain Eq. (3). Thus we have acquired a self-consistent mathematical description.

5. Gravitational collapse

Can we distinguish a collapsing self-gravitating cloud from a turbulent region within which the Jeans mass is not reached? We here take a simulation of driven hydrodynamic turbulence in which self-gravity is switched on after a steady driven state has been reached (Model D2 from Klessen et al. 2000). The particular parameters chosen are shown in the caption to Fig. 9.

The number and distribution of shock speeds is not particularly different from the equivalent non-gravity numerical

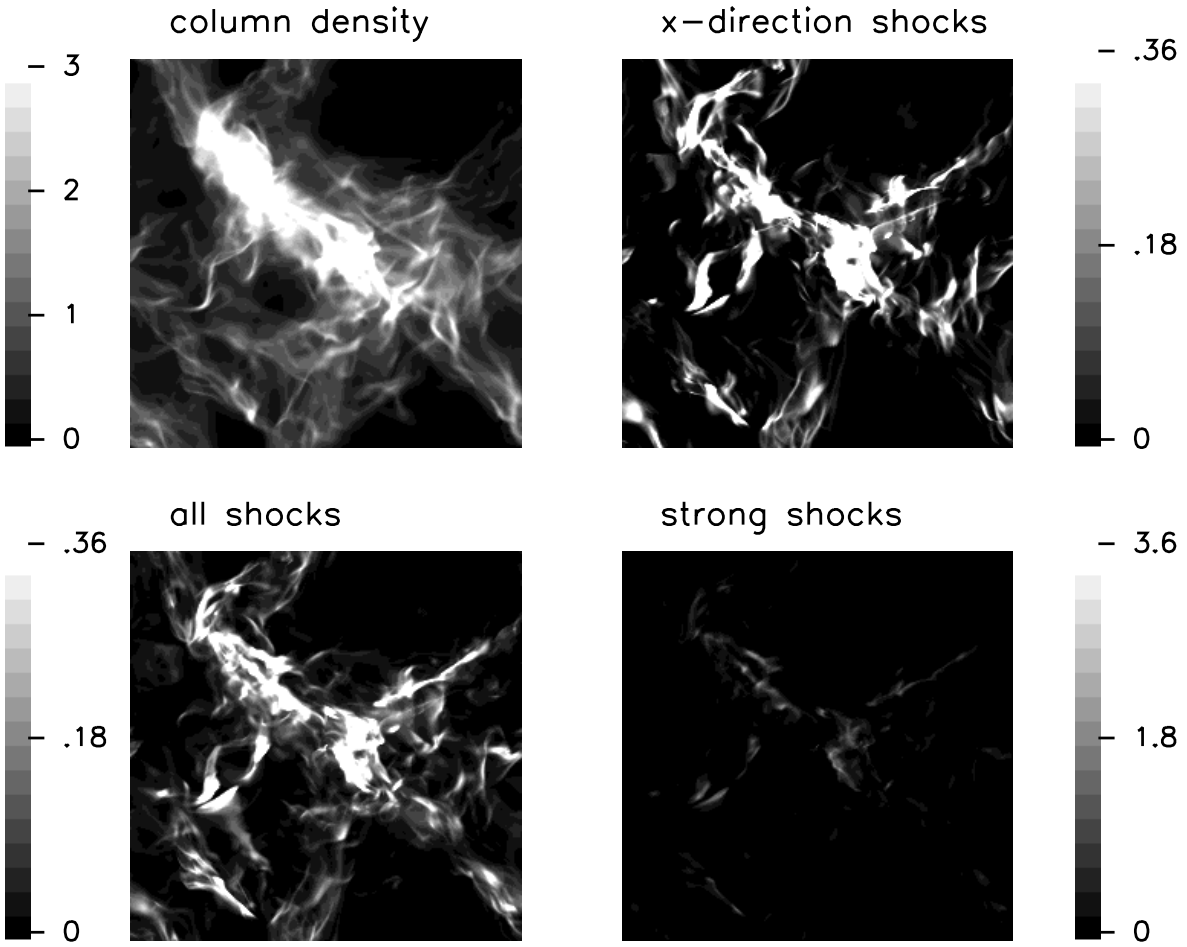

Fig. 6. Maps of the column and power dissipated from driven turbulence integrated through the cube along the z-direction. The run is D1 of Klessen et al. 2000, at time t = 2, just before self-gravity was switched on. The long wavelength driving ($k_{max} = 2$) generates a large cloud structure visible in the column density, the density projected onto the x-y plane. The energy dissipated in the shocks (1) just in the x-direction, (2) in all directions and (3) in just the strongest shocks, are displayed as indicated. The column density is expressed relative to the average (initial) value, and the power loss per image pixel has been amplified by a factor of 128^2.

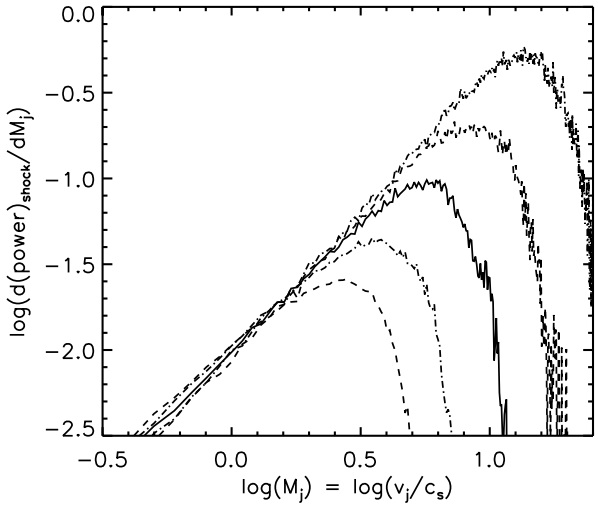

Fig. 7. The rate of energy dissipation from shocks with jump Mach number M_j. The log-log plot demonstrates that power law relation. The 5 curves correspond to the simulations shown in Fig. 1 with increasing input powers dE/dt = (0.1, 0.3, 1, 3, 10).

experiment. The power-law section is limited, consistent with other low wavenumber simulations (see Fig. 2).

In stark contrast, the dissipated energy transforms from the typical non-gravity case (upper box of Fig. 10) to one dominated by a few accretion shocks (lower box of Fig. 10). A relatively small number of well-defined shocks generates strong individual signatures. These shocks are of typical cloud speeds but are strongly dissipative because they propagate into very dense regions.

The distribution of the shocks at time t = 6 is displayed in Fig. 11. The elongated cloud at time t = 2 (Fig. 6) has now collapsed into narrow filaments and cores. There is high shock dissipation around the collapsing cores although other strong shocks are still quite widespread. The code does not distinguish between a shock and a collapsing flow. The artificial viscosity prescription treats all converging flow regions as dissipative. Nevertheless, a collapsing flow does physically dissipate its energy as it shocks onto a growing core. Hence the dynamical evolution is correctly modelled. The surface brightness of the shocks is, of course, limited by the grid resolution. The high

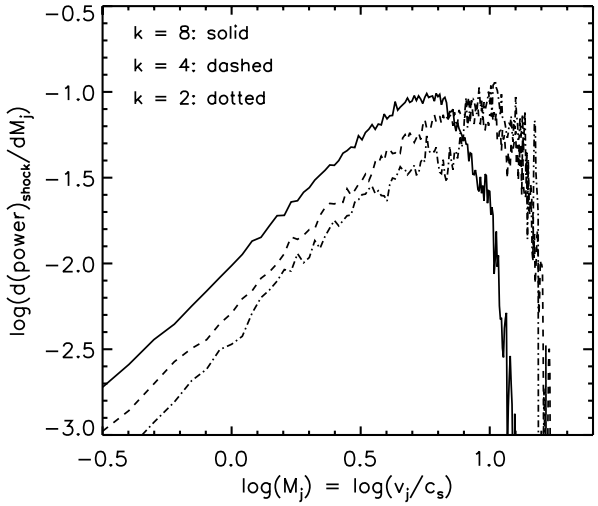

Fig. 8. The distributions of the rate of energy dissipation for the three indicated maximum wavenumbers, corresponding to the number distributions shown in Fig. 2.

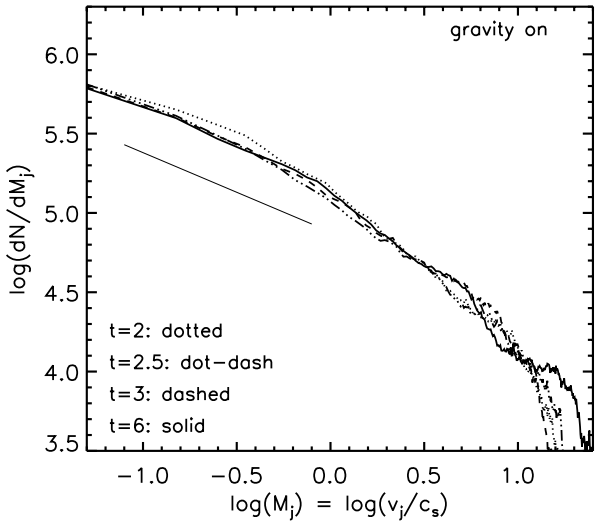

Fig. 9. The distribution of shocks in driven turbulence with gravity. The initial rms speed is $9.9c_s$, $\dot{E} = 0.4$, wavenumber $k = 2$ and the density is chosen to be 0.125 (total mass of unity in the periodic box). The gravitational constant is set to unity. The gravity is switched on after the driven turbulence is well established at time $t = 2$. The turbulent Jeans mass is 3.2 (see Klessen et al. 2000).

SPH resolution, however, verifies that the general properties are realistic (Klessen et al. 2000). A new problem arising in the shock analysis is that a single converging flow onto a core may actually be a double shock layer. We would here record this as a single shock in the counting procedure and in Fig. 10. We have not tried to correct for this.

6. Interpretation

Turbulence has proven easy to interpret, but the interpretations have been hard to prove. Our aim here is limited to answer: why a universal inverse square root power law? Supersonic turbulence

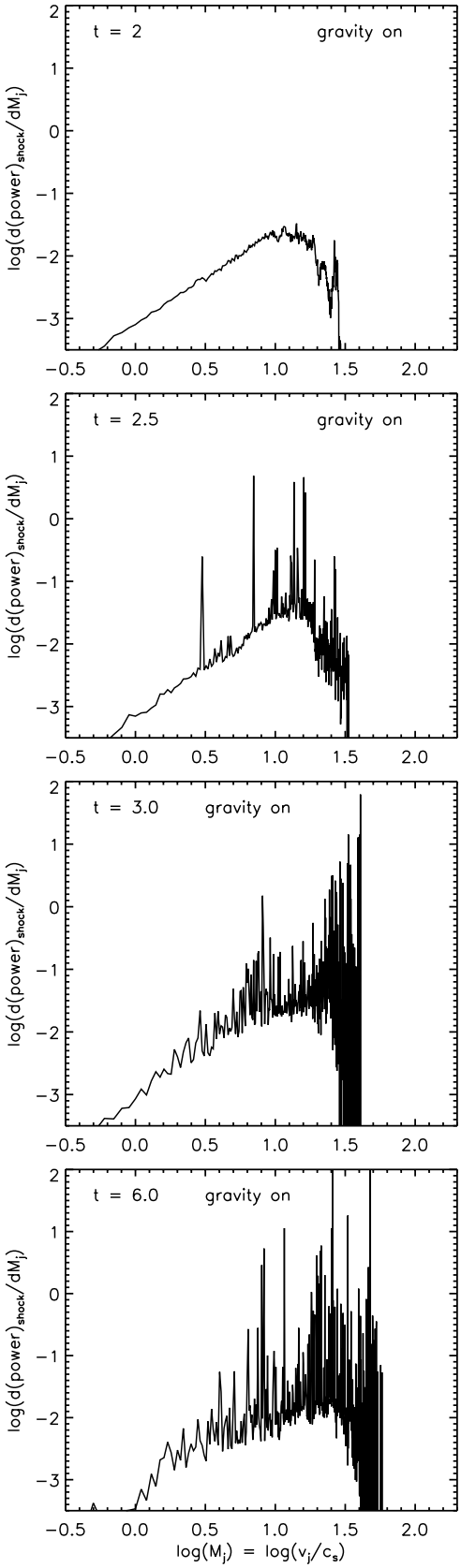

Fig. 10. The power dissipated by shocks in driven turbulence with gravity at the four indicated times. Gravity is just switched on at the time $t = 2$. The parameters are as in Fig. 9.

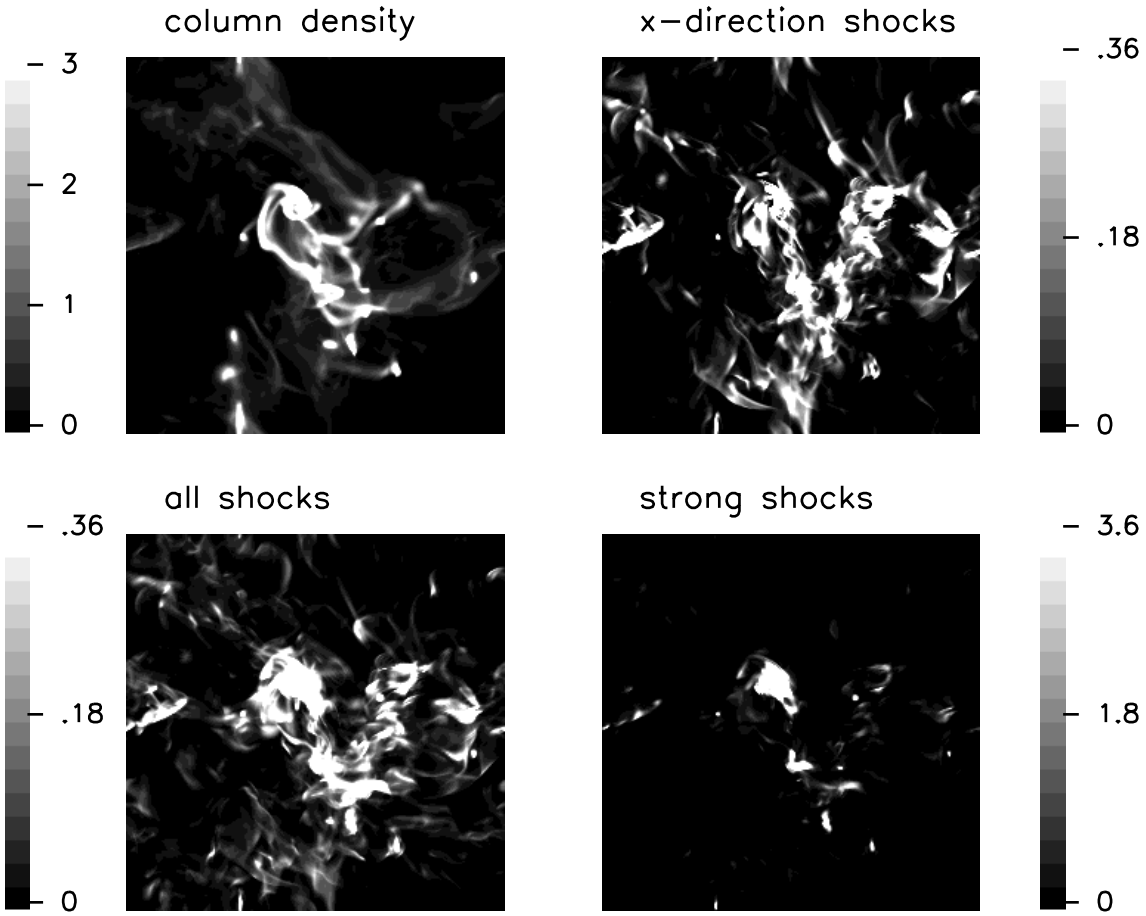

Fig. 11. Maps of the column and power dissipated in driven turbulence with gravity at the time t = 6. Note the grey scaling allow a direct comparison with Fig. 6. The elongated cloud at time t = 2 has now collapsed into narrow filaments and cores.

possesses simplifying characteristics which we here employ to understand the shock distribution.

First, it is significant that the flow is dominated by the integrated number and power of the high-speed shocks at the knee in the shock jump distributions. These shocks are generated by the driver and propagate at high speed into the fluid. In contrast, a shock from the power-law section plays a passive rôle: when overtaken by a strong shock, its strength decays according to the speed and density of the oncoming material. Hence the mean lifetime, τ, of a shock layer, and hence of the shock momentum, is a constant, independent of its own absolute speed, v. Expressed mathematically, for a steady state, this yields

$$\frac{\partial}{\partial v}\left[\frac{\partial N}{\partial v}\frac{1}{\tau}\right] = 0, \tag{8}$$

from which we find the distribution of absolute shock speeds (i.e. the speed of the layers within the box) is $\partial N/\partial v = constant$. This is confirmed from the simulations - Fig. 12 shows that, below the high-speed knee, the distribution of absolute velocities within the shocks is indeed independent of the absolute speed.

The relationship between the absolute speed, v, and the jump speed, v_j, for the ensemble of shocks is expected to resemble that of Burger's turbulence (Paper 1, see also Gotoh & Kraichnan 1993). The steepening of these independently-moving shocks is proportional to the absolute speed simply because higher amplitude waves produce stronger shocks, whereas low amplitude waves can only lead to weak jumps. Secondly, the higher amplitudes imply that the velocity gradients are also steeper. Hence the material swept up into a shock is from a wider region which possesses a larger velocity difference. These two linear effects lead to a relationship for the ensemble shock jump and absolute speeds of the form $v_j \propto v^2$. This is the essence of mapping closure theory, which then uses this relationship to transform initial Gaussian distributions into exponentials (Chen et al. 1989, Kraichnan 1990). Here, we transform the distribution of absolute shock speeds generated by the uniform driving, to obtain

$$\frac{\partial N}{\partial v_j} \propto v_j^{-1/2}. \tag{9}$$

This agrees with the numerical experiments. Note that the result depends on the nature of the driving: uniform driving produces strong shocks locally which then propagate through the ambient medium. In contrast, a white-noise driver would continually create weak small-scale turbulence throughout the space and might thus produce, for example, some other power-law behaviour.

We found here that the high-velocity tail is somewhat steeper than Gaussian. A similar result has been obtained for other types of turbulence, with the same form occurring, $\exp(-v_j^3)$, as un-

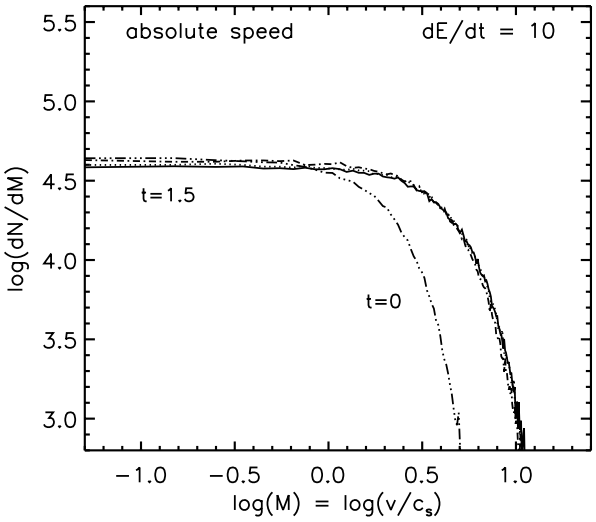

Fig. 12. The remarkable number distribution of shock absolute speeds in uniform driven turbulence for the four times from t=0 to t=1.5. The absolute speed is defined as the average speed in the x-direction within a region of converging flow along the x-axis. So defined, we do not have to contend with the shock direction or with determining the 3-D shock structure, but retain the vital information for modelling.

covered here (see Gotoh & Kraichnen 1998). This is due to the Gaussian forcing being modified by the high dissipation rates at these speeds.

The total energy 'radiated' in the shocks can be found on integrating Eq. (7) over the jump Mach Number. This yields $P = 0.669\,\dot{E}$. The remaining injected energy is also lost in the shocks where numerical diffusion is, of course, strong. As shown in Table 1 of Paper 1, we expect approximately 0.68 of the energy to be radiated in the shocks. Hence, the description of driven turbulence is fully consistent.

7. Conclusions

We have analysed numerical simulations of uniformly driven supersonic, magnetohydrodynamic and self-gravitating turbulence. Below a critical jump speed, we find a power law distribution of fast shocks with the number of shocks inversely proportional to the square root of the shock jump speed. Hence, unlike the decaying case, the driven case possesses an 'inertial range' of shock strengths. This range is, however, dynamically passive, being mediated by strong shocks injected at a higher knee in the distribution. The knee is mainly responsible for the dissipation of energy, and thus the power-law range may only have a weak observational signature. This will be explored in the following paper of this series.

These results contrast with the exponential distribution and slow shock dissipation associated with decaying turbulence described in Paper 1.

A strong magnetic field does not alter the shape of the shock number distributions. It enhances the shock number transverse to the field direction at the expense of parallel shocks. The distribution of parallel shocks is, however, extended to higher jump speeds. Transverse waves thus appear to find support in the magnetic pressure.

A simulation with self-gravity demonstrates the development of a number of highly dissipative accretion shocks. These shocks are rare and are not apparent in the number distributions. The shock number distribution demonstrates a gradual curvature rather than a power-law. This implies that high-speed shocks can be maintained by gravitational acceleration.

Finally, we have shown how the power-law behaviour may arise. No substantial theory has been developed to predict this inverse square root law. The power law is closely related to the distribution in absolute shock speeds, which is shown to be flat. The particular power law is predicted to depend on the type of driver.

The energy is dissipated in shocks mainly associated with the denser regions of the clouds formed by the large scale wave motions. Numerous other shocked regions are scattered throughout. Very strong shocks are associated with the collapsing cores in the self-gravitating case.

Our results must be considered within the context of the imposed models. While turbulence has been pinned down in many studies, further studies have simply extended the number of pins required. Extensions to this work include: (1) the shock distributions corresponding to non-uniform drivers, (2) the spatial propagation of turbulent energy and (3) the observable signatures: the spectral energy distributions derived from the shock distributions,

Acknowledgements. MDS benefitted greatly from the hospitality of the Max-Planck-Institut für Astronomie. We thank R. Klessen and E. Zweibel for advice and discussions. Computations were performed at the MPG Rechenzentrum Garching. M-MML holds a CAREER fellowship from the US National Science Foundation, grant number AST 99-85392.

References

Chen H., Chen S., Kraichnan R.H., 1989, Phys. Rev. Lett. 63, 2657
Eislöffel J., Smith M.D., Davis C.J., 2000, A&A in press
Falgarone E., Lis D.C., Phillips T.G., et al., 1994, ApJ 436, 728
Franco J., Carramiñana A., 1999, Interstellar Turbulence. CUP, Cambridge
Gotoh T., Kraichnan R.H., 1993, Phys. Fluids A, 5, 445
Gotoh T., Kraichnan R.H., 1998, Phys. Fluids 10, 2859
Heitsch F., Mac Low M.-M., Klessen R.S., 2000, ApJ submitted
Klessen R.S., Heitsch F., Mac Low M.-M., 2000, ApJ 535, 887
Kraichnan R.H., 1990, Phys. Rev. Lett. 65, 575
Mac Low M.-M., 1999, ApJ 524, 169
Mac Low M.-M., Ossenkopf V., 2000, A&A 353, 339
Mac Low M.-M., Burkert A., Klessen R., Smith M.D., 1998, Phys. Rev. Lett. 80, 2754
Mac Low M.-M., Smith M.D., Klessen R., Burkert A., 1999, Ap&SS 246, 195
Padoan P., Juvela M., Bally J., Nordlund A., 1998, ApJ 504, 300
Porter D.H., Pouquet A., Woodward P.R., 1994, Phys. Fluids 6, 2133
Smith M.D., Mac Low M.-M., Zuev J.M., 2000, A&A 356, 287 (Paper 1)
Vázquez-Semadeni E., Passot T., Pouquet A., 1996, ApJ 473, 881
von Hoerner S., 1962, In: Woltjer L. (ed.) The distribution and motion of interstellar matter in galaxies. W.A. Benjamin, New York, p. 193